Conformational dynamics of a G-protein α subunit is tightly regulated by nucleotide binding

David Goricanec[a,b,c], Ralf Stehle[b,c], Pascal Egloff[d], Simina Grigoriu[e], Andreas Plückthun[d], Gerhard Wagner[e,1], and Franz Hagn[a,b,c,e,1]

[a]Institute for Advanced Study at the Department of Chemistry, Technische Universität München, 85747 Garching, Germany; [b]Center for Integrated Protein Science Munich at the Department of Chemistry, Technische Universität München, 85747 Garching, Germany; [c]Institute of Structural Biology, Helmholtz Zentrum München, 85764 Neuherberg, Germany; [d]Department of Biochemistry, University of Zurich, CH-8057 Zurich, Switzerland; and [e]Department of Biological Chemistry and Molecular Pharmacology, Harvard Medical School, Boston, MA 02115

Contributed by Gerhard Wagner, March 21, 2016 (sent for review November 19, 2015; reviewed by Heidi E. Hamm and Lewis E. Kay)

Heterotrimeric G proteins play a pivotal role in the signal-transduction pathways initiated by G-protein–coupled receptor (GPCR) activation. Agonist–receptor binding causes GDP-to-GTP exchange and dissociation of the Gα subunit from the heterotrimeric G protein, leading to downstream signaling. Here, we studied the internal mobility of a G-protein α subunit in its apo and nucleotide-bound forms and characterized their dynamical features at multiple time scales using solution NMR, small-angle X-ray scattering, and molecular dynamics simulations. We find that binding of GTP analogs leads to a rigid and closed arrangement of the Gα subdomain, whereas the apo and GDP-bound forms are considerably more open and dynamic. Furthermore, we were able to detect two conformational states of the Gα Ras domain in slow exchange whose populations are regulated by binding to nucleotides and a GPCR. One of these conformational states, the open state, binds to the GPCR; the second conformation, the closed state, shows no interaction with the receptor. Binding to the GPCR stabilizes the open state. This study provides an in-depth analysis of the conformational landscape and the switching function of a G-protein α subunit and the influence of a GPCR in that landscape.

GPCR | NMR | SAXS | structure | signaling

Heterotrimeric G proteins are localized at the inner leaflet of the plasma membrane where they convey signals from cell-surface receptors to intracellular effectors (1). Heterotrimeric G proteins consist of two functional units, an α subunit (Gα) and a tightly associated βγ complex. The Gα subunit harbors the guanine nucleotide-binding site. In the inactive GDP-bound state, the Gα subunit is associated with the βγ complex. Exchange of GDP for GTP on the Gα subunit, triggered by interaction with the agonist-bound G-protein–coupled receptor (GPCR), results in a conformational change leading to GDP release and ultimately to GTP binding and subunit dissociation. The complexity of the mechanism by which a GPCR activates the Gα subunit based on available crystal structures has been discussed recently (2, 3). Both the Gα subunit and the βγ subunit interact with downstream effectors and regulate their activity. The intrinsic GTP hydrolysis of the Gα subunit returns the protein to the GDP-bound state, thereby increasing its affinity for the Gβγ subunit, and the subunits reassociate (Fig. 1*A*), ready for interaction with the agonist-bound GPCR. Throughout this cycle, the Gα subunit is engaged in specific interactions with the GPCR and/or the βγ subunit that stabilize the flexible parts of the protein, e.g., its switch regions. Only the GTP-bound form is stable enough to mediate downstream signaling.

Crystallographic (4–9), biochemical (10), and biophysical (11–13) studies have elucidated details of the conformational states of the Gα subunit during the GTPase cycle. The Gα subunit has two structural domains, a nucleotide-binding domain (the Ras-like domain) and a helical domain (the α-H domain) that partially occludes the bound nucleotide (Fig. 1*A*). Because of this steric consideration, nucleotides can be released only upon at least partial opening of the two domains. The Ras-like domain is associated with the membrane surface through N-terminal myristoylation, and its position is further restricted by interaction with the βγ complex and the GPCR. The helical domain is connected to the nucleotide-binding domain through two flexible linkers, and linker 1 (switch I) undergoes conformational changes upon receptor binding (12). The relative orientation of these two subdomains has been investigated previously at lower resolution by double electron–electron resonance (DEER) spectroscopy (13–15). One of these studies (15) also used extensive molecular dynamics (MD) simulations to monitor conformational changes within the Gα subunit. In these calculations the authors identified large conformational changes taking place in the microsecond time scale.

To determine experimentally the changes in the relative orientation and dynamics of the two subdomains of the Gα subunit in its apo form and upon binding to GDP and GTP, we performed a thorough NMR spectroscopic characterization of an inhibitory Gα subunit, Gαi1. We combined our NMR experiments with small-angle X-ray scattering (SAXS), circular dichroism (CD), and fluorescence spectroscopy to gain detailed insights into the conformational states of Gαi1 along the nucleotide-binding trajectory. In addition, we performed Carr–Purcell–Meiboom–Gill (CPMG) relaxation dispersion experiments, MD simulations, and 2D NMR transverse relaxation optimized spectroscopy (TROSY) experiments to monitor the dynamics of Gαi1 in the minute-to-microsecond time scale in the apo form and in complex with different nucleotides. The results show that Gαi1 adopts a more open conformation in the apo and GDP-bound forms, but its conformation is fairly compact and rigid in complex with GTP analogs. The degree of Gα domain opening as determined here is less pronounced than shown in a

Significance

G proteins are molecular switches for cellular signaling induced by G-protein–coupled receptor activation. The Gα subunit is the central timer of signal transduction regulated by GTP hydrolysis, which returns the system to its inactive state. Although previous work has characterized the structural states of Gα during the GTPase cycle, we show here that Gα is highly dynamic in the apo and GDP-bound states but in complex with GTP is completely rigid and is locked in a defined domain orientation. These insights help demonstrate that the conformational plasticity of G proteins is a central feature of their switching functionality.

Author contributions: F.H. designed research; D.G., R.S., P.E., S.G., and F.H. performed research; F.H. analyzed data; and A.P., G.W., and F.H. wrote the paper.

Reviewers: H.E.H., Vanderbilt University; and L.E.K., University of Toronto.

The authors declare no conflict of interest.

Data deposition: The NMR chemical shift assignments of Gαi1 in the apo form and in complex with GDP and GMP-PNP have been deposited at the Biological Magnetic Resonance Bank data bank (accession codes 30077, 30078, and 26746, respectively). The structural models of Gαi1 in the apo form and in complex with GDP have been deposited at the Protein Data Bank (PDB) database (PDB ID codes 5JS7 and 5JS8). The structural model of the GMP-PNP–bound form is almost identical to an existing crystal structure (rmsd of 0.88 Å) and therefore has not been deposited in the PDB.

[1]To whom correspondence may be addressed. Email: franz.hagn@tum.de or gerhard_wagner@hms.harvard.edu.

This article contains supporting information online at www.pnas.org/lookup/suppl/doi:10.1073/pnas.1604125113/-/DCSupplemental.

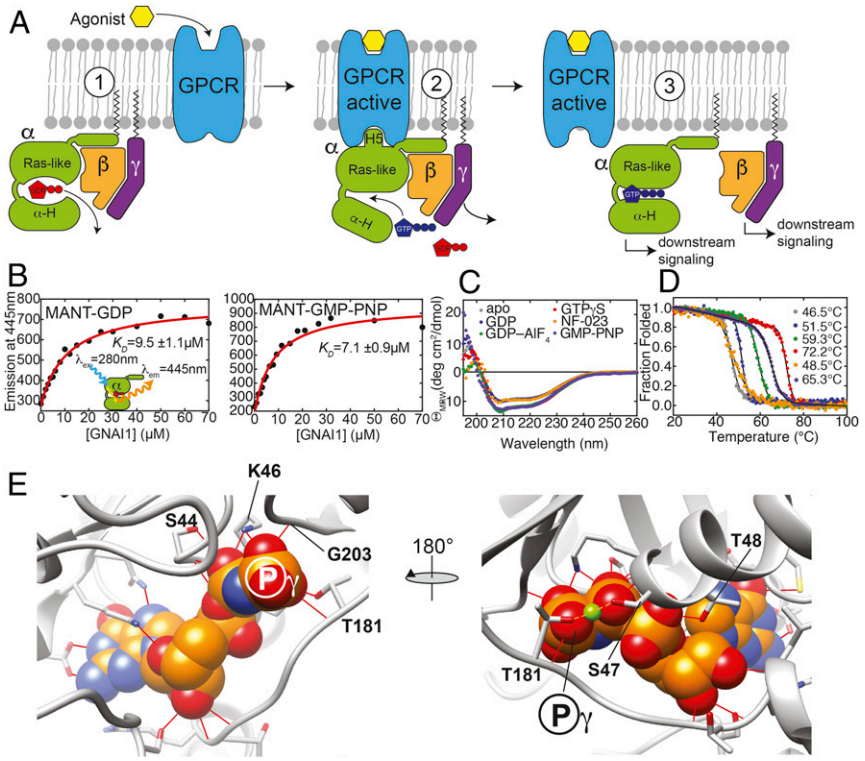

Fig. 1. Ligand binding and thermal stability assays of an inhibitory Gαi1 subunit. (*A*) Mechanism of G-protein activation by a GPCR. A GPCR ligand binds to the receptor and induces its active conformation, i.e., binding to a heterotrimeric G protein located at the intracellular side of the cell membrane. This activation stimulates a conformational change within the Gαi1 subunit leading to the exchange of bound GDP for GTP and to the subsequent dissociation of the heterotrimer and downstream signaling. (*B*) FRET-based nucleotide-binding assay using fluorescently (MANT)-labeled GDP and GMP-PNP. Intrinsic tryptophan residues in the protein were excited at 280 nm, and the FRET signal at 445 nm was monitored upon the stepwise addition of Gαi1. (*C* and *D*) CD spectra (*C*) and CD-detected thermal melting curves (*D*) of Gαi1Δ31 bound to various ligands. (*E*) Binding mode of GMP-PNP to Gαi1. Residues engaged in additional hydrogen bonds (red lines) occurring only in the GMP-PNP–bound form are highlighted.

recent GPCR-stimulatory heterotrimeric G protein complex structure (3) but is in line with previous electron paramagnetic resonance (EPR) studies (13) at lower resolution and with MD simulations (15). In contrast to those studies, here we present structural models of the Gα conformational states at a per-residue resolution based on various structural methods. Furthermore, we provide detailed insights into the functional dynamics of Gαi1 extracted from CPMG relaxation dispersion and 2D TROSY NMR experiments. These data show that the Gα subunit is dynamic in the apo and GDP-bound form but is rigid in complex with GTP. We also show that the GPCR-binding ability of Gα correlates positively with the degree of conformational plasticity. Thus, this study describes previously unknown dynamical properties of the Gα subunit in solution and in the conformational states associated with GPCR binding.

Results

Active Gαi1 Can Be Produced in *Escherichia coli* for NMR Structural Studies. To produce human Gαi1 (UniProt accession no. P63096) for biophysical studies and NMR spectroscopy, we constructed a fusion protein containing Gαi1 and GB1 (protein G B1 domain) serving as an expression and solubility tag (16) during expression in *E. coli*. Low-temperature cell growth and application of low concentrations of isopropyl β-D-1-thiogalactopyranoside (IPTG) for induction (see *Methods* and previous protocols in ref. 17) allowed us to obtain 5–10 mg of active Gαi1 per liter of cell culture. Purified protein was free of bound GDP as probed by ^{1}H NMR spectroscopy (Fig. S1). Initial NMR experiments performed with full-length Gαi1 resulted in poor spectral quality, so we designed a truncated variant lacking the N-terminal 31 residues (Gαi1Δ31). The deleted part of the protein is not resolved in the crystal structure [Protein Data Bank (PDB) ID code: 1cip (18)] and is unfolded in solution as shown here by NMR and elsewhere (19). This truncated protein variant resulted in high-quality NMR spectra as probed with 2D [^{15}N,^{1}H]-TROSY and TROSY for rotational correlation times (TRACT) experiments (Fig. S2). To validate the nucleotide-binding activity of Gαi1Δ31, we used FRET assays with methylanthraniloyl (MANT)-labeled nucleotides (MANT-GDP and MANT–GMP-PNP) (Fig. 1*B*). Upon excitation of protein tryptophan side chains at 280 nm, the emitted light leads to excitation of the MANT moiety and finally emission at 445 nm. Subsequent titration of protein to a 1-μM MANT–nucleotide solution led to a proper binding curve that permitted the extraction of binding constants in the order of 10 μM with slightly tighter binding of the GTP analog. Next, we characterized the secondary structure, content, and thermal stability of Gαi1 in the presence of different nucleotides and inhibitors (Fig. 1*C*). The minima in the CD signal of Gαi1Δ31 at 208 and 222 nm, indicative of the α-H secondary structure, are markedly increased in the presence of GTP analogs and are less pronounced in complex with GDP and the G-protein inhibitor NF-023. In line with these findings, the thermal stability of these complexes as monitored with CD is highest with guanosine 5′-*O*-(3-thiotriphosphate (GTPγS) and lowest in the apo form, indicating a strong stabilizing effect of GTP analogs. These differences can be partly explained by the formation of additional hydrogen bonds between the γ-phosphate of the GTP analog and Gαi1Δ31 (Fig. 1*D* and Fig. S3). We investigated the structural and internal mobility details of these different structural states using solution NMR spectroscopy.

Gαi1 Displays Ligand-Dependent Changes as Probed with NMR Chemical Shift Perturbations. To characterize the structure and dynamics within Gαi1 upon binding to various nucleotides, we produced U-[^{2}H,^{13}C,^{15}N]–labeled Gαi1Δ31 and prepared a sample with a protein concentration of ∼250 μM, either in the apo form or in the presence of 3 mM GDP, guanosine 5′-[β,γ-imido]triphosphate (GMP-PNP), or GTPγS. We performed the following TROSY-based 3D triple-resonance NMR experiments (20) on these samples: HNCO, HN(CA)CO, HNCA, HN(CO)CA, HNCACB, and 3D-^{15}N–edited TROSY-NOESY. All 3D experiments were recorded with Poisson-gap nonuniform sampling (NUS) data acquisition (21) and iterative soft threshold (IST) reconstruction (22). We could obtain backbone assignments of 89% (288/323) of the residues for the GMP-PNP–bound (Fig. 2*A*), 88% (284/323) for the GTPγS-bound, 78% (252/323) for the GDP-bound, and 77% (259/323) for the apo state. Chemical shift-based estimation of the secondary structure based on differences in random coil chemical shifts in Cα and Cβ

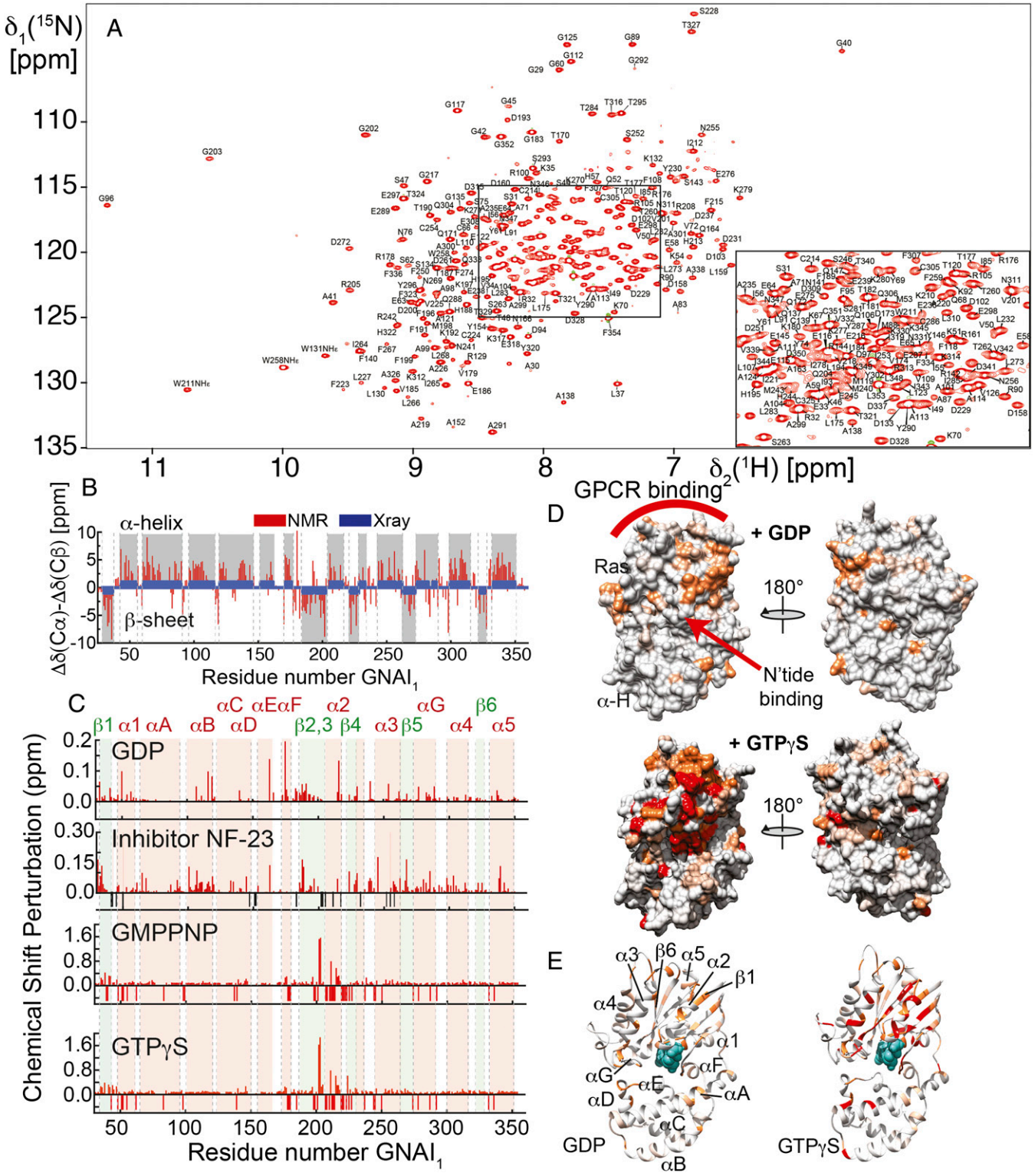

Fig. 2. NMR assignment and mapping of binding sites of Gαi1. (*A*) 2D [^{15}N,^{1}H]-TROSY spectra of Gαi1Δ31 in complex with the nonhydrolyzable GTP analog GMP-PNP. Around 85% of all backbone resonances could be assigned, as labeled. (*B*) Secondary chemical shift of Gαi1Δ31 plotted against residue number. Positive and negative values indicate α-helical and β-sheet conformation, respectively. As a comparison, the secondary structure elements in the crystal structure (PDB ID code: 1cip) are shown as blue bars. (*C*) [^{15}N,^{1}H]-averaged chemical shift perturbations within Gαi1Δ31 upon the addition of various ligands. Negative black and red bars indicate resonances disappearing or reappearing, respectively, upon ligand binding. (*D*) Chemical shift perturbations mapped onto the structure of Gαi1 color-coded in orange and red according to the positive and negative bars in *C*. (*E*) Cartoon representation of Gαi1 bound to GDP and to GTPγS color-coded according to NMR chemical shift perturbations. Structural elements within Gαi1 are labeled. Nucleotides are shown as green spheres.

nuclei (23) correlates well with the secondary structure elements in the crystal structure of Gαi1 in complex with GMP-PNP (PDB ID code: 1cip) (Fig. 2*B*). We further analyzed the NMR spectral changes in Gαi1Δ31 upon the addition of various nucleotides and the Go/i-selective Suramin-based small-molecule inhibitor NF-023 (Fig. 2*C*) (24). The data show that GDP induces relatively small (up to 0.15 ppm) chemical shift perturbations within Gαi1Δ31. These chemical shift changes cluster specifically to the Ras-like domain with little effect on the helical domain (gray and orange coloring in Fig. 2 *D* and *E*). The inhibitor induces a similar pattern of chemical shift changes but in addition leads to the disappearance of 18 resonances, most likely because of exchange broadening (negative black bars in Fig. 2*C*) located around the nucleotide-binding site and along the GPCR-binding site in the Ras domain. In contrast, the addition of GTP analogs (GMP-PNP and GTPγS) leads to the appearance of 38 additional resonances (red negative bars in Fig. 2*C* and red color in Fig. 3 *D* and *E*), which again are clustered around the nucleotide-binding site and all over the Ras-domain of Gαi1. The appearance of additional resonances points toward the quenching of exchange processes and a more rigid structure of Gαi1Δ31 in the GTP-bound form, in line with crystallographic studies (5) in which the electron density of parts of the Ras domain could not be observed in the GDP-bound form, presumably because of increased flexibility (Fig. S3). Furthermore, GTP analogs induce larger chemical shift perturbations than GDP clustered around the docking site of the two subdomains (Fig. 2 *C* and *D*). Regions around residues 204–217 and residues 233–239 are not resolved in the crystal structures of Gαi1 in the GDP-bound form but are visible in the complex structure with GMP-PNP (Fig. S3).

Gαi1 Interacts with an Activated GPCR in Phospholipid Nanodiscs. We next studied the interaction between uniformly ^{2}H,^{15}N-labeled Gαi1Δ31 with a thermostabilized (25, 26), signaling-competent (27) variant of rat neurotensin receptor subtype 1 [HTGH4 L167R (28)], which was purified from *E. coli* as described previously (27, 29) and then incorporated in phospholipid nanodiscs (30, 31). The binding process was monitored by 2D-[^{15}N,^{1}H]-TROSY experiments with ^{2}H,^{15}N-labeled Gαi1Δ31 in the apo, GDP-, or GMP-PNP–bound forms. We recorded NMR experiments with Gαi1Δ31 samples alone and after the addition of empty nanodiscs assembled with 1-Palmitoyl-2-oleoyl-sn-glycero-3-phosphocholine (POPC) lipids and membrane scaffold protein 1D1 (MSP1D1) and finally in complex with nanodiscs containing neurotensin-activated HTGH4 (Fig. 3 and Fig. S4).

Differences in NMR resonance positions in these experiments were used to calculate chemical shift perturbations of Gαi1Δ31 upon GPCR binding (color coding in Fig. 3). We observe a weak effect between empty nanodiscs and Gαi1Δ31 that was more pronounced in the apo and GDP-bound states and was weaker in the closed GMP-PNP–bound state. Sites in Gαi1Δ31 affected by binding to the phospholipid bilayer are located in sheets β2 and β3, in switch III, and around helix αG and helix α5 (Fig. 3*A*). However, the addition of GPCR-containing nanodiscs induced more pronounced chemical shift perturbations in the fast chemical-exchange regime within Gαi1Δ31 in the apo and GDP-bound states but not in the GMP-PNP–bound state (Fig. 3*B*). These effects are most prominent for the apo state and are located in sheets β1, β2, β3, and β5, helix αG, helix α4, sheet β6, and the C-terminal helix α5 in the Ras domain. The C-terminal helix previously has been shown to undergo translational and rotational motion upon GPCR binding and represents one of the main sites of interaction with the activated GPCR (3, 11). This interaction might be more pronounced in the presence of the Gβγ subunit and with myristoylated Gα.

Relative Gαi1 Domain Orientation Is Dependent on Nucleotide Binding. To obtain further structural insights about the orientation of the two subdomains in Gαi1, the Ras-like domain and the helical

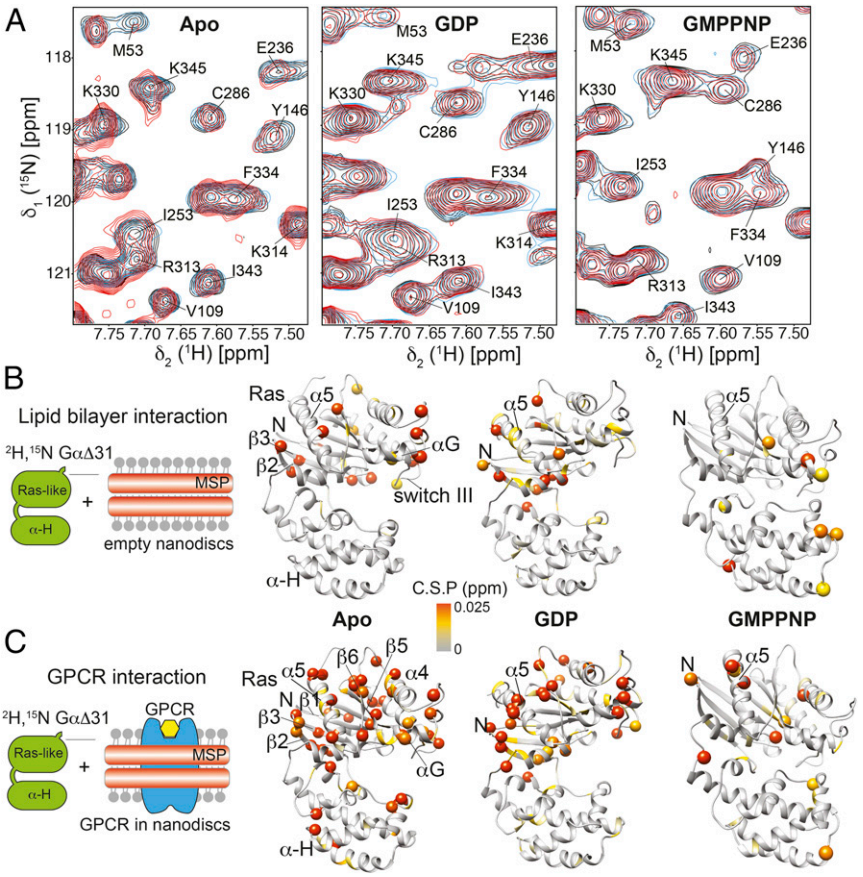

Fig. 3. Interaction between Gαi1Δ31 and a GPCR in phospholipid nanodiscs. (*A*) 2D [^{15}N,^{1}H]-TROSY experiments were used to extract chemical shift changes of 50 μM ^{2}H,^{15}N-labeled Gαi1Δ31 (black spectra) in the apo, GDP-bound, and GMP-PNP–bound forms upon the addition of an equimolar amount of the neurotensin-bound activated neurotensin-1 receptor variant HTGH4 L167R (28) in phospholipid nanodiscs (red spectra) or 50-μM empty nanodiscs as a reference (blue spectra). Chemical shift perturbations are mapped onto the structure and are color-coded according to the chemical shift perturbations (C.S.P.) bar. (*B*) Empty nanodiscs induce moderate chemical shift perturbations on Gαi1Δ31 that are more pronounced in the open apo and GDP-bound forms than in the closed GMP-PNP–bound form. (*C*) In contrast, the chemical shift perturbations induced by GPCR-containing nanodiscs clearly cluster within the Ras domain around helix 5, the main site of interaction with the GPCR. These effects are most pronounced in the apo state and are absent in the closed GMP-PNP–bound state. MSP, membrane scaffold protein.

domain, we performed SAXS experiments on the apo, GDP-, and GTPγS-bound forms of Gαi1Δ31 (Fig. 4*A* and Table 1). SAXS data yield the overall shape and radius of gyration of the biomolecule of interest.

For an independent determination of the domain orientation in more structural detail, we recorded NMR TROSY and semi-TROSY experiments using Pf1 phage–induced aligned Gαi1Δ31 samples to extract backbone amide residual dipolar couplings (RDCs). In the semi-TROSY experiment, the signal position is shifted in the ^{1}H dimension by the ^{1}H,^{15}N coupling constant plus the residual dipolar coupling ($^{1}J + {}^{1}D$) compared with the TROSY experiment. RDCs are well suited for determining the relative orientation of protein domains. The RDC data were used to refine the structural models obtained with SAXS. As can be seen in Fig. 4*B*, the overall correlation between the experimental RDCs and the RDCs back-calculated from the refined structures is very good, yielding correlation coefficients of at least 0.95. The fitted components of the alignment tensor are shown in each subpanel. The resulting overall structural model fitted to the SAXS-based envelope in each case is shown in Fig. 4*C*, and the corresponding structural statistics are reported in Table 2. The main differences between these structures are slight changes in distance and rotational angle between the two subdomains. These changes in subdomain orientation lead to an overall opening of the nucleotide-binding site in the apo state and the GDP-bound state compared with the closed GTP-bound conformation. The GTP-bound model is basically identical to an existing crystal structure of GMP-PNP–bound Gα [PDB ID code 1cip (18)] in which the two domains are docked tightly against each other and the secondary structure elements are formed at the interface. This structural picture is in line with the thermal stabilities measured with CD spectroscopy in which the GTP-bound form shows an ∼25 °C higher melting point than the apo and GDP-bound forms, indicating better domain docking in the presence of GTP. To probe the degree of freedom in relative domain orientation, we further used MD simulations of apo-Gαi1Δ31 at 37 °C. In Fig. 4*D*, the distance between the centers of mass (COM) of the Ras and α-H domains is plotted against simulation time, and representative snapshots are shown above the plot. These simulations show that Gαi1 is very dynamic, with distances between the two COM ranging from 25–32 Å, leading to varying positions of the two domains with respect to each other. Thus, imperfections in correlation between the SAXS envelopes and the refined structures are most likely caused by the inherent dynamics of the two domains.

This aspect was investigated further by fluorescence spectroscopy with MANT-labeled nucleotides (MANT-GDP and –GMP-PNP). We first probed the environment of MANT-GDP and

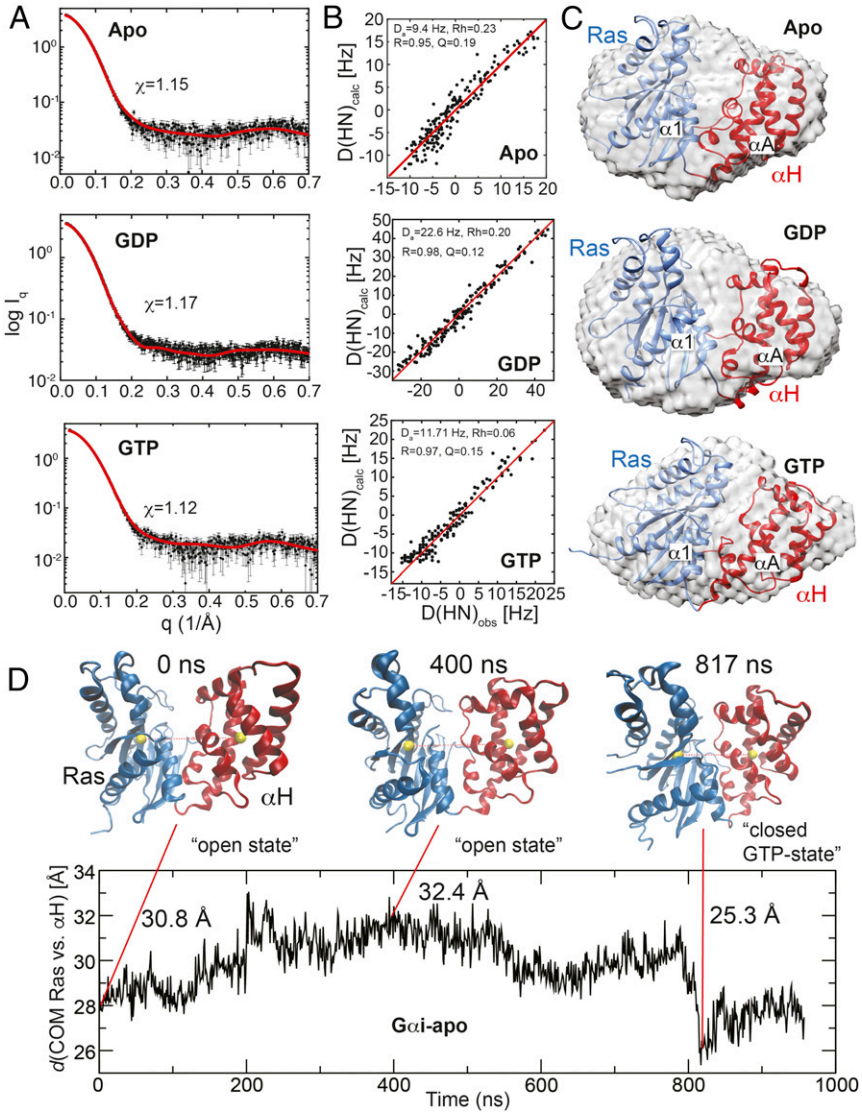

Fig. 4. Structural changes within Gαi1 in the apo and GDP- or GTPγS-bound forms using SAXS and NMR RDCs. (*A*) SAXS data and back-calculated scattering profiles of Gαi1Δ31 in the apo, GDP-, or GTPγS-bound forms. (*B*) Structural models derived from SAXS experiments were refined further with amide proton-nitrogen (HN)-RDCs obtained with 8 mg/mL Pf1 phage-aligned Gαi1Δ31 in the apo and GDP- or GTPγS-bound form. Correlation and quality factors of the agreement between back-calculated and experimental RDCs are shown. (*C*) Structural models obtained after the two-step refinement in each case. The apo and GDP-bound forms adopt a more open conformation than the GTP-bound form. (*D*) MD simulation of apo-Gαi1Δ31 at 37 °C. The distance between the COM (center of mass) of the Ras and α-H domains (yellow spheres) is plotted against simulation time, and structural snapshots at the indicated times are shown.

Table 1. SAXS data collection and data analysis statistics

	Gαi1-GTPγS	Gαi1-GDP	Gαi1-apo
Data collection			
Instrument	BIOSAXS1000	BIOSAXS1000	BIOSAXS1000
Beam geometry	Point	Point	Point
Wavelength, Å	1.54187	1.54187	1.54187
Q range, $Å^{-1}$	0.09–0.7	0.09–0.7	0.09–0.7
Exposure time, h	0.5	0.5	0.5
Concentration range, mg/mL	2–10	2–10	2–10
Temperature, °C	20	20	20
Structural parameters*			
R_g, Å [from P(r)]	22.08 ± 0.05	21.93 ± 0.05	21.98 ± 0.04
R_g, Å [from Guinier]	22.1 ± 0.2	22.6 ± 0.2	22.6 ± 0.2
Dmax, Å	72.5	69.4	67.8
Porod volume estimate, $Å^3$	54,600	53,089	55,469
Molecular mass determination			
Molecular mass M_r, Porod volume	44	43	45
Calculated monomeric M_r from sequence	37	37	37
Software used			
Primary data reduction	SAXSLab v3.0.1r1	SAXSLab v3.0.1r1	SAXSLab v3.0.1r1
Data processing	Primus, Coral (atsas 2.5.0–2)	Primus, Coral (atsas 2.5.0–2)	Primus, Coral (atsas 2.5.0–2)

*Reported for the 10-mg/mL measurement.

MANT–GMP-PNP provided by Gαi1Δ31 using this assay. The fluorescence spectra of MANT are sensitive to the hydrophobicity of the surrounding environment. As a reference, we measured a spectrum of MANT–GMP-PNP in buffer solution. Without bound protein, the two MANT nucleotides give identical spectra. As can be seen in Fig. 5*A*, there are pronounced changes in the fluorescence emission spectra of MANT-GDP and MANT–GMP-PNP after binding to Gαi1Δ31. The emission intensity of MANT–GMP-PNP is higher, and its maximum is blue-shifted compared with MANT-GDP, a strong indication that Gαi1Δ31 entraps MANT–GMP-PNP more tightly than the GDP adduct. To probe direct contact between the MANT-nucleotides and the protein, we used FRET; we irradiated the protein at 280 nm and recorded emission spectra from 350–600 nm (Fig. 5*B*). The FRET peak of the bound MANT dye appears around 425 nm. Because of the lack of protein in the reference MANT–GMP-PNP sample in buffer, no FRET signal was observed. The Gαi1-MANT-GDP sample showed only slightly increased FRET efficacy. In contrast, the FRET emission of the Gαi1–MANT–GMP-PNP sample was around three times higher than that of the MANT–GDP sample, again indicating tight binding between MANT–GMP-PNP and the protein.

Table 2. Structural statistics of Apo, GDP-, and GTP-bound Gαi1

	Apo	GDP	GTPγS
Deviations from restraints and idealized geometry			
NH RDCs*	Rms = 2.27 Hz	Rms = 2.53 Hz	Rms = 2.09 Hz
	R = 0.952, Q = 0.186	*R* = 0.991, Q = 0.083	*R* = 0.974, Q = 0.149
	A = 9.4 Hz, Rh = 0.23	A = 22.6 Hz, Rh = 0.20	A = 11.05 Hz, Rh = 0.09
SAXS $\chi^{2\dagger}$	1.15	1.17	1.12
Bonds, Å	$2.60e^{-3} \pm 3.11e^{-5}$	$3.49e^{-3} \pm 1.71e^{-4}$	$2.51e^{-3} \pm 4.87e^{-5}$
Angles, °	0.67 ± 0.01	0.96 ± 0.05	0.66 ± 0.01
Impropers, °	1.87 ± 0.05	3.61 ± 0.34	1.57 ± 0.04
Ramachandran map analysis, %‡			
Most favored	89.1	82.8	89.7
Additionally allowed	9.4	14.9	8.5
Generously allowed	1.5	1.7	0.6
Disallowed	0.0	0.7	1.2
Structural statistics§			
Backbone rmsd, Å	0.66 ± 0.11¶	0.43 ± 0.29¶	0.53 ± 0.06¶
	0.35 ± 0.05#	0.19 ± 0.05#	0.32 ± 0.04#
	0.31 ± 0.07‖	0.17 ± 0.05‖	0.26 ± 0.05‖
Heavy atom rmsd, Å	0.82 ± 0.10¶	0.46 ± 0.28¶	0.71 ± 0.08¶
	0.49 ± 0.04#	0.24 ± 0.05#	0.45 ± 0.05#
	0.52 ± 0.07‖	0.23 ± 0.05‖	0.47 ± 0.07‖

*Determined with the program Pales (36).
†Calculated with the SAXS module in Chimera using the FoXS server.
‡Calculated with ProcheckNMR (37).
§Rmsd analysis of the best 20 total energy structures:
¶All structured parts (residues 33–348).
#Ras domain only (residues 33–56,184–348).
‖α-H domain only (residues 62–177).

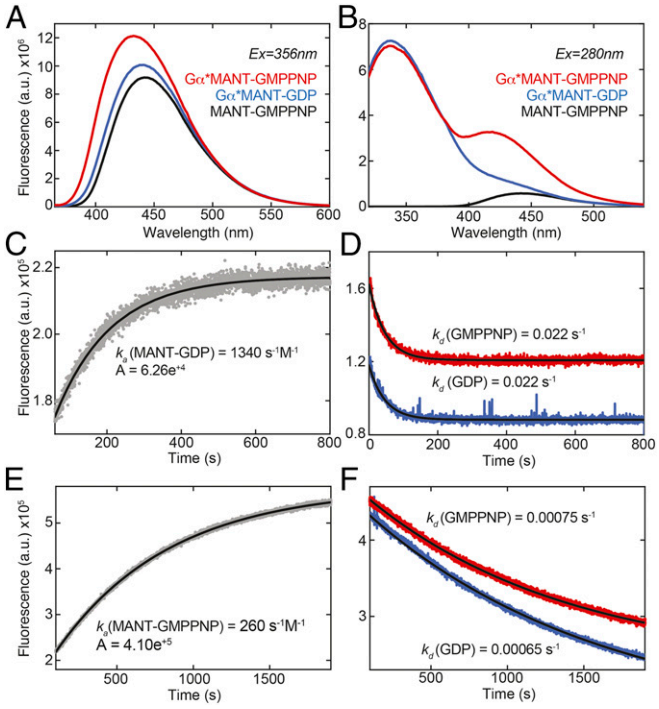

Fig. 5. Nucleotide-binding properties and exchange kinetics monitored with fluorescence spectroscopy. (*A*) Fluorescence spectra of the free and Gαi1Δ31-bound MANT-labeled nucleotides obtained by direct excitation of the dye at 356 nm. The fluorescence intensity and emission maximum increase subsequently from the free to the GMP-PNP–bound form. (*B*) FRET spectra of the MANT-labeled nucleotides obtained by excitation of tryptophan side chains at 280 nm. (*C*) Association kinetics of 5 μM MANT-GDP to 20 μM Gαi1Δ31. (*D*) Dissociation kinetics of the same sample upon the addition of 50 μM GDP or GMP-PNP, respectively. (*E*) Association kinetics of MANT–GMP-PNP to Gαi1Δ31. (*F*) Dissociation of the complex by the addition of an excess of GDP or GMP-PNP is much slower than in the MANT-GDP case. Calculated K_d values for the interaction between Gαi1Δ31 and MANT-GDP and MANT–GMP-PNP are 16 and 3 μM, respectively.

We next investigated the kinetic properties of nucleotide association and dissociation. We used MANT-labeled nucleotides and observed the buildup of FRET intensity over time after the addition of Gαi1Δ31. As shown in Fig. 5*C*, the association of 5 μM MANT-GDP with 20 μM Gαi1Δ31 is a single-exponential process with an observed association rate constant (k_{on}) of 1,340 1/(s·M). This complex can be dissociated rapidly, and rebinding is prevented by a 10-fold excess of unlabeled GDP or GMP-PNP, following the same observed rate constant (k_{off}) of 0.022/s (Fig. 5*D*), yielding a calculated K_d ($K_d = k_{off}/k_{on}$) of 16 μM. The same association–dissociation experiment conducted with MANT-labeled GMP-PNP yields an observed association rate constant (k_{on}) of 260 1/(s·M) (Fig. 5*E*), which is considerably slower than the GDP association rate and most likely is caused by structural rearrangements within Gαi1 to accommodate the GTP fully. Dissociation of this tight complex is slow and is dependent on the nucleotide type used as a competitor. Dissociation in the presence of excess GDP is characterized by a k_{off} of 0.00065/s, whereas with GMP-PNP as a competitor slightly faster dissociation is observed with a k_{off} of 0.00075/s (Fig. 5*F*). The calculated K_d for GMP-PNP is 3 μM. These experiments confirm not only that the Gαi1-GTP complex is tighter than the GDP complex but also that it is characterized by markedly reduced association and very slow dissociation rates.

Nucleotide Binding Strongly Alters Gαi1 Dynamics. To investigate the nucleotide-dependent dynamics of the Gαi1 subunit in the nanosecond-to-picosecond, millisecond-to-microsecond, and slower time scales, we performed various NMR experiments in the apo, GDP-, and GTPγS-bound forms. First, $\{^1H\}^{15}N$-heteronuclear NOE experiments, reporting on dynamics in the nanosecond-to-picosecond time scale, were recorded on the three samples (Fig. S5). These experiments showed that GMP-PNP–bound Gαi1Δ31 is very rigid throughout the sequence. In contrast, the apo or GDP-bound forms show greater flexibility at the N-terminal β1-strand and more pronounced fluctuations in dynamics throughout the protein. To probe dynamics in the millisecond-to-microsecond time scale, we performed ^{15}N and ^{13}C CPMG relaxation dispersion experiments, which are particularly suitable for probing conformational changes such as protein-folding events (32) and motions associated with enzyme catalysis (33). Initially, we recorded ^{15}N CPMG relaxation dispersion experiments on the apo, GDP-, and GTPγS-bound forms on backbone amide resonances in the protein. The resulting data indicate chemical exchange in the apo and GDP-bound but not in the GTPγS-bound form, where only flat dispersion profiles could be observed, as shown for His188 in Fig. 6*A*. The dispersion profiles of the apo and GDP-bound forms differ slightly, indicating alterations in the chemical-exchange properties of these two states. To evaluate the chemical-exchange processes of the apo and GDP sample further, we made use of the enhanced NMR signal intensity of methyl groups suitable for studying dynamics of large protein systems (34). 2D $[^{13}C,^1H]$-heteronuclear multiple quantum coherence (HMQC) experiments of selectively Ileδ1, Leuδ2, Valγ2, Alaβ $^1H,^{13}C$-methyl-, and otherwise $^2H,^{12}C,^{15}N$-labeled Gαi1Δ31 were of excellent quality and thus are suitable for extracting chemical shift perturbations upon ligand binding and for conducting ^{13}C-CPMG relaxation dispersion experiments (Fig. S6). We therefore measured single-quantum ^{13}C-CPMG relaxation dispersion experiments at static magnetic field strengths of 600 and 900 MHz and obtained dispersion profiles of sufficient quality for data analysis (Fig. 6 *B* and *C*), except for parts that are severely exchange-broadened in the apo and GDP-bound states (sheet 1, helix 2), as labeled in Fig. S6*A*. Methyl groups in Gαi1Δ31 showing chemical exchange in the millisecond-to-microsecond time scale are color-coded in the apo and the GDP-bound form, respectively (Fig. 6 *B* and *C*). Residues involved in fast exchange, residues involved in slow exchange, and residues that are severely exchange-broadened are shown as blue, red, and yellow spheres, respectively. Regions exhibiting chemical exchange cluster around the nucleotide- and GPCR-binding sites but also are present in the α-H domain. Switch regions (switches I, II, and III) are exchange-broadened or show slow chemical exchange in the apo and GDP-bound forms. Overall, differences in exchange rates between the apo and the GDP-bound form can be detected only in the Ras domain, where the average exchange rate drops from ∼900 to 740 Hz. Dynamics of the α-H domain is not affected by GDP binding, indicating that binding of GDP to the Ras domain does not induce its docking to the α-H domain. This observation is in line with thermal denaturation analyses of Gαi1Δ31 in both forms that showed only a slight increase in the transition temperature in the GDP-bound form versus the apo form (Fig. 1*C*). We further analyzed populations of the ground and excited states in the millisecond-to-microsecond time scale for helix 5, the main interaction site with GPCRs, in the apo and GDP-bound forms in more detail. A comparison of the two forms shows that the population of the ground state (p_A) of residues in and surrounding helix 5 is around 5% lower in the GDP-bound state than in the apo state. Therefore, we speculate that GDP stabilizes the excited state, which possibly is similar the GTP-bound closed state in which helix 5 is tightly bound to the Ras domain. Possible effects of the G-βγ subunit on the overall dynamics of the Gα subunit remain to be shown in future studies.

A closer look at the 2D TROSY spectra of the different states provides additional evidence for the existence of two conformational states of the Gα subunit in very slow exchange (Fig. 7*A*). We observed a second signal set for a subset of residues located in the Ras domain in both the apo and GDP-bound forms but not in the

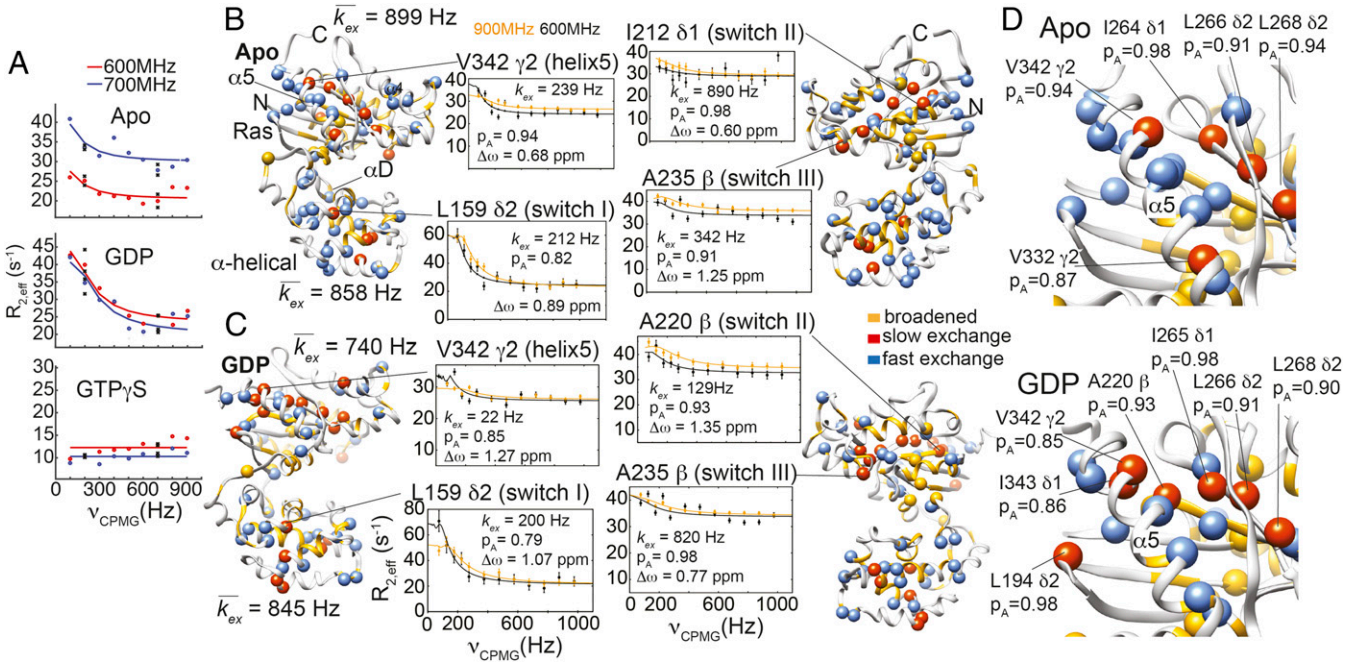

Fig. 6. Millisecond-to-microsecond dynamics of Gαi1Δ31. (*A*) ^{15}N-CPMG relaxation dispersion profiles recorded at magnetic field strengths of 600 and 700 MHz. His188 of Gαi1 is shown as an example to illustrate the effect of nucleotides on the inherent dynamics of the protein. (*B* and *C*) Millisecond-to-microsecond dynamics of Gαi1 in the apo (*B*) and GDP-bound (*C*) forms extracted from ^{13}C-CPMG relaxation dispersion experiments measured at 600 (black) and 900 MHz (orange) proton frequency, respectively. Residues in fast exchange are shown in blue, residues in slow exchange are shown in red, and severely exchange broadened residues are shown in yellow. (*D*) Populations of the ground state in the apo and GDP-bound state of helix 5 and nearby residues. The addition of GDP induces a slightly higher population in the excited state.

closed GTP-bound state. The α-H domain was not affected, as shown exemplarily by the single signal of the amide resonance of Gly112. All other resonances in Fig. 7*A* are located in the Ras domain and give rise to a second signal set in the apo and GDP-bound form, except for F191, which shows one signal in the apo form and two in the GDP-bound form. The resonance position that most likely corresponds to the GTP-bound closed conformation is indicated by the intersection of the horizontal and vertical dashed lines, implying that the closed species is also populated in the apo and GDP-bound forms. Analysis of the relative peak intensities suggests that GDP binding leads to a markedly higher population in the excited state than present in the apo form. Overall, these effects cluster to the Ras domain in general and to helix 5 in particular, and the chemical shift differences between the two states are more pronounced in the GDP-bound form than in the apo form (Fig. 7*B*). Helix 5 is the main interaction site with a GPCR, and inherent changes in its conformation therefore are crucial for the binding event. We analyzed the relative heights of the corresponding NMR signals and calculated the populations of the ground state, which are ∼65% for the apo form and ∼35% for the GDP-bound form (Fig. 7*C*, *Left*). Next we investigated the influence of an activated GPCR on the relative population of the ground state. We used nanodiscs incorporating rat neurotensin receptor-1 variant HTGH4 L167R (28), performed 2D [^{15}N,^{1}H]-TROSY experiments, and analyzed the change in NMR signal intensity of the ground and excited states. The population of the ground state in the apo form is increased by 5% upon GPCR binding; this increase is less pronounced than the 20% increase determined for the GDP-bound state (Fig. 7*C*, *Right*). These experiments show that interaction with an activated GPCR is mediated by the Gα ground state. The addition of nucleotides leads to the preferred or complete formation of a second conformation. Binding of a GPCR enhances the population of the ground state, and this effect is more pronounced with the GDP-bound Gα subunit, thus favoring the nucleotide-exchange process. As shown in Fig. 3, the closed Gα-GTP complex does not interact with a GPCR, and, in turn, the apo state shows the most pronounced binding effects upon the addition of a GPCR. We assume that the presence of the Gβγ subunit will lead to a more defined conformational state of the Gα subunit in complex with GDP, and the GPCR might shift the conformational equilibrium toward a low-affinity ground state that also is present in apo Gα. However, because of current limitations in investigating such a large complex with solution-state NMR, this question remains to be addressed in future studies.

Discussion

In this study our goal was to conduct a detailed survey of the structure and internal mobility of Gαi1 in complex with different nucleotides and an activated GPCR in phospholipid nanodiscs by solution NMR, CD, and fluorescence spectroscopy, SAXS, and MD simulations. We were able to assign the NMR backbone resonances of apo Gαi1Δ31, as well as the GDP- and GTP-bound forms. These NMR assignments could be used in combination with SAXS experiments to extract differences in chemical shift and to obtain NMR RDCs for the refinement of the relative orientations of the Ras and α-H domains of Gαi1 in the various ligand-bound forms. The results revealed a nucleotide-dependent conformational change in Gαi1, in which GTP induces a very tight and stable domain-docked state (Fig. 4). In contrast, in the apo form both domains adopt a more open topology that permits binding of GDP or GTP to the nucleotide-binding site.

The relative changes in domain orientation of Gαi1 domains shown here are less pronounced than described in a previous crystal structure of a stimulatory G protein in complex with β2-adrenergic receptor (3), which also contained a nanobody bound to the Gα–Gβ interface, but are in better agreement with more recent studies based on molecular modeling and DEER spectroscopy (13–15). In addition to these earlier studies, we were able to probe the dynamics and the populations of the associated conformational states. We could clearly show that the populations of these states change upon the addition of GDP and that binding of GTP completely abolished internal dynamics as

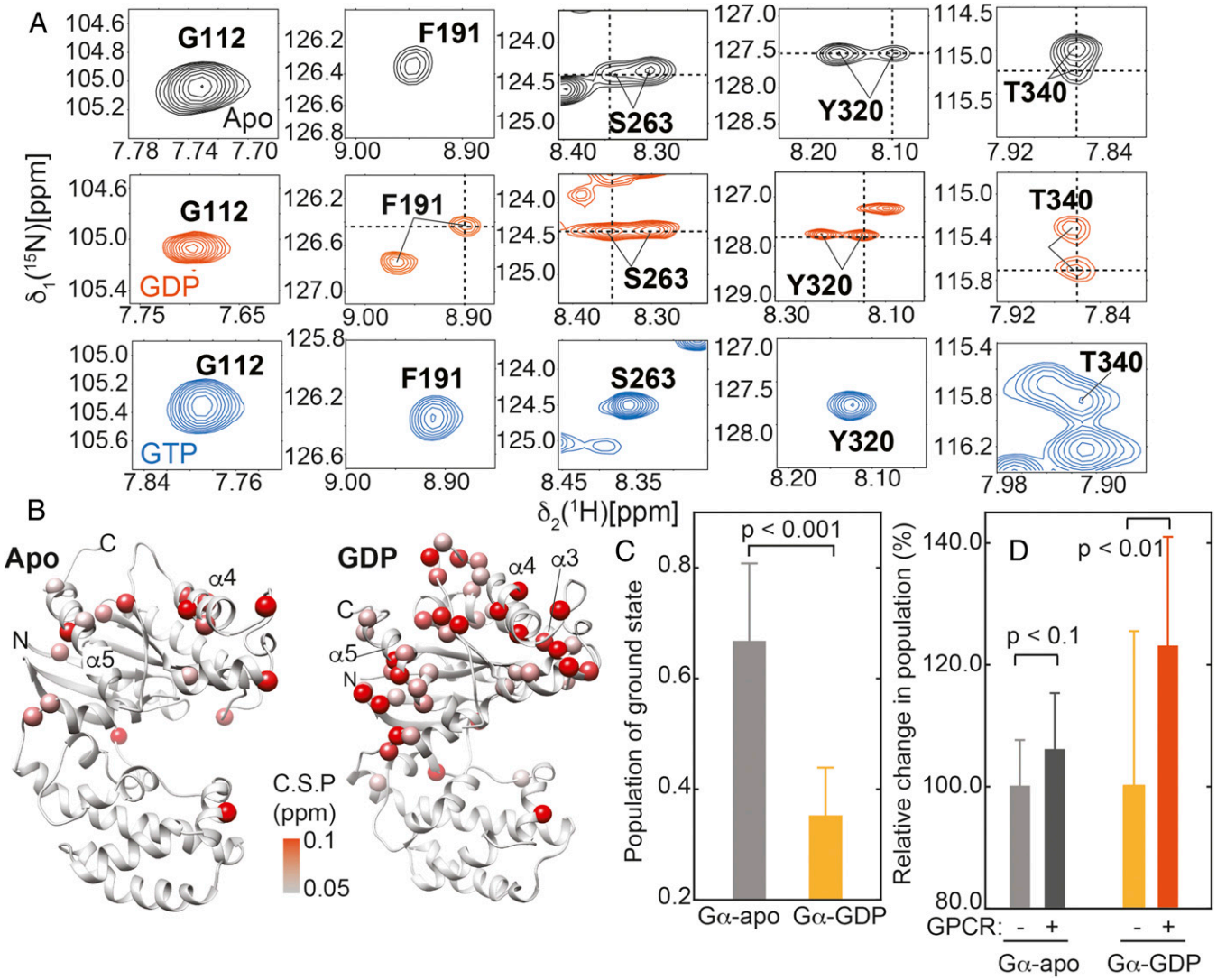

Fig. 7. Gα conformational states are modulated by nucleotide and GPCR binding. (*A*) Regions of 2D [^{15}N,^{1}H]-TROSY spectra of Gα in the apo (black), GDP-bound (orange), and GMPPNP-bound (blue) states. The apo and GDP-bound forms show two conformational states in slow exchange (longer than seconds) that give rise to the appearance of a second signal set in the NMR experiment. The GMP-PNP–bound state exists in one defined conformation and consequently gives rise to only one set of NMR signals. (*B*) C.S.P. (color coding: gray to red) between the two Gα NMR signal sets are mapped onto the structure. These data show that only the Ras domain is affected and that chemical shift perturbations are more pronounced in the GDP-bound form. (*C*) Population of the ground state in the apo and GDP-bound forms. The addition of GDP leads to a significantly decreased population of the ground state. (*D*) The influence of GPCR-binding on the population of the ground state. This influence is less pronounced in the apo state than in the GDP-bound state. The minus and plus signs indicate the absence or presence, respectively, of nanodisc-incorporated and -activated neurotensin receptor variant HTGH4 L167R.

measured by our assays. We could detect these effects in the millisecond-to-microsecond as well as in the minute-to-second time scale. Of particular interest is the finding that the major conformational state of the apo state is less populated in the GDP-bound state and is completely absent in the GTP-bound state. In addition, the appearance of this ground state correlates well with the binding behavior of Gα to an activated GPCR. The relative intensity of NMR signals corresponding to this state increases when Gα is in complex with a GPCR. This result suggests that only one conformational species of Gα, highly populated in the apo form but also present to some extent in the GDP-bound form, is capable of high-affinity binding to an activated GPCR. The addition of GDP pushed the equilibrium toward the excited (lower-affinity) state. This tendency can be reverted by binding to a GPCR, providing evidence that a GPCR promotes nucleotide exchange by stabilizing the nucleotide-free conformation of a Gα subunit. In contrast, the GTP-bound form is present in a single closed and rigid conformation whose population cannot be altered by a GPCR because of a lack of interaction. These findings demonstrate a tight interplay between nucleotide and GPCR binding mediated by allosteric structural changes. Residues that show two conformations in slow exchange cluster to the upper face of the Ras domain (Fig. 7*B*), and basically the same interface is affected by GPCR binding (Fig. 3). Conformational changes in the Gα subunit upon binding to a GPCR have been reported in a previous EPR study (12) and crystal structure (3). These reports suggest that helix 5 must undergo a translational and rotational motion to interact with the receptor. A more recent MD simulation study provides further insights, suggesting that this motion is restricted by GDP binding (15). Interaction with a GPCR leads to a disorder-to-order transition within the C-terminal part of helix 5, as recently summarized for existing G-protein structures (2).

Our findings can be included in the well-explored activation cycle of a heterotrimeric G protein mediated by GPCR in which, as a first step, GDP-bound heterotrimeric G protein interacts with an activated receptor. The receptor then pushes the Gα

conformation slightly toward a low-affinity state for GDP. The GDP-bound Gα subunit is quite flexible, and we speculate that even in the complex with the βγ subunit there would be enough conformational space to mediate such slight structural changes. The resulting apo heterotrimeric G protein eventually binds to GTP, leading to subunit dissociation and loss of affinity with the receptor. The change in affinity in the Gα subunit can be directly correlated with its conformational states. The apo form showing the highest affinity for the receptor is present mostly in the ground state, as determined by NMR (Fig. 7). In the GDP-bound form, both, the ground and the excited state occur, resulting in a reduced affinity for the receptor. Finally, in complex with GTP, the Gα subunit lacks any dynamics and exists exclusively in the excited state, thus losing affinity with the GPCR.

Methods

Protein production was done in *E. coli* as described previously (17). Proteins were purified with NiNTA and size-exclusion chromatography. We used a FRET assay to extract binding affinities between Gα and MANT-labeled GDP or GMP-PNP nucleotides. Secondary structure estimation and thermal stability screens of Gα preparations were done with CD spectroscopy. NMR assignment experiments with U-^{2}H,^{13}C,^{15}N–labeled Gα were recorded in a NUS manner (21, 22). Dynamical parameters were extracted from ^{15}N- and ^{13}C-CPMG relaxation dispersion experiments (35). Structural changes upon nucleotide binding were detected with SAXS, and the conformational flexibility of Gα was further determined with MD simulations. More experimental details can be found in *SI Methods*.

ACKNOWLEDGMENTS. We thank Dr. Gianluigi Veglia (University of Minnesota) for providing a ^{13}C-CPMG relaxation dispersion pulse program, Dr. Sven Brüschweiler (Harvard Medical School) for help with the ^{15}N-CPMG relaxation dispersion setup, and the Leibniz Supercomputing Centre of the Bavarian Academy of Sciences and Humanities for providing and supporting the computing infrastructure essential for this work. All SAXS data were recorded at the Brown University Structural Biology Core Facility. This work received support from a Human Frontier Science Program long-term fellowship (LT000297/2011-L) and the Institute for Advanced Study of the Technical University of Munich (TUM-IAS) funded by the German Excellence Initiative and the European Union Seventh Framework Program under Grant 291763, as well as the Center for Integrated Protein Science Munich (CIPSM) and the Helmholtz Center Munich (to F.H.). G.W. was supported by National Institutes of Health Grants GM047467 and EB002026. G.W. and A.P. were supported by the Human Frontier Science Program Grant RGP0060/2016.

1. Gilman AG (1987) G proteins: Transducers of receptor-generated signals. *Annu Rev Biochem* 56:615–649.
2. Flock T, et al. (2015) Universal allosteric mechanism for Gα activation by GPCRs. *Nature* 524(7564):173–179.
3. Rasmussen SG, et al. (2011) Crystal structure of the β2 adrenergic receptor-Gs protein complex. *Nature* 477(7366):549–555.
4. Coleman DE, et al. (1994) Crystallization and preliminary crystallographic studies of Gi alpha 1 and mutants of Gi alpha 1 in the GTP and GDP-bound states. *J Mol Biol* 238(4):630–634.
5. Coleman DE, Sprang SR (1998) Crystal structures of the G protein Gi alpha 1 complexed with GDP and Mg2+: A crystallographic titration experiment. *Biochemistry* 37(41):14376–14385.
6. Lambright DG, Noel JP, Hamm HE, Sigler PB (1994) Structural determinants for activation of the alpha-subunit of a heterotrimeric G protein. *Nature* 369(6482):621–628.
7. Noel JP, Hamm HE, Sigler PB (1993) The 2.2 A crystal structure of transducin-alpha complexed with GTP gamma S. *Nature* 366(6456):654–663.
8. Wall MA, et al. (1995) The structure of the G protein heterotrimer Gi alpha 1 beta 1 gamma 2. *Cell* 83(6):1047–1058.
9. Lambright DG, et al. (1996) The 2.0 A crystal structure of a heterotrimeric G protein. *Nature* 379(6563):311–319.
10. Higashijima T, Ferguson KM, Sternweis PC, Smigel MD, Gilman AG (1987) Effects of Mg2+ and the beta gamma-subunit complex on the interactions of guanine nucleotides with G proteins. *J Biol Chem* 262(2):762–766.
11. Oldham WM, Van Eps N, Preininger AM, Hubbell WL, Hamm HE (2006) Mechanism of the receptor-catalyzed activation of heterotrimeric G proteins. *Nat Struct Mol Biol* 13(9):772–777.
12. Oldham WM, Van Eps N, Preininger AM, Hubbell WL, Hamm HE (2007) Mapping allosteric connections from the receptor to the nucleotide-binding pocket of heterotrimeric G proteins. *Proc Natl Acad Sci USA* 104(19):7927–7932.
13. Van Eps N, Oldham WM, Hamm HE, Hubbell WL (2006) Structural and dynamical changes in an alpha-subunit of a heterotrimeric G protein along the activation pathway. *Proc Natl Acad Sci USA* 103(44):16194–16199.
14. Alexander NS, et al. (2014) Energetic analysis of the rhodopsin-G-protein complex links the α5 helix to GDP release. *Nat Struct Mol Biol* 21(1):56–63.
15. Dror RO, et al. (2015) Signal transduction. Structural basis for nucleotide exchange in heterotrimeric G proteins. *Science* 348(6241):1361–1365.
16. Zhou P, Wagner G (2010) Overcoming the solubility limit with solubility-enhancement tags: Successful applications in biomolecular NMR studies. *J Biomol NMR* 46(1):23–31.
17. Greentree WK, Linder ME (2004) Purification of recombinant G protein alpha subunits from Escherichia coli. *Methods Mol Biol* 237:3–20.
18. Coleman DE, Sprang SR (1999) Structure of Gialpha1.GppNHp, autoinhibition in a galpha protein-substrate complex. *J Biol Chem* 274(24):16669–16672.
19. Maly J, Crowhurst KA (2012) Expression, purification and preliminary NMR characterization of isotopically labeled wild-type human heterotrimeric G protein αi1. *Protein Expr Purif* 84(2):255–264.
20. Salzmann M, Pervushin K, Wider G, Senn H, Wüthrich K (1998) TROSY in triple-resonance experiments: New perspectives for sequential NMR assignment of large proteins. *Proc Natl Acad Sci USA* 95(23):13585–13590.
21. Hyberts SG, Takeuchi K, Wagner G (2010) Poisson-gap sampling and forward maximum entropy reconstruction for enhancing the resolution and sensitivity of protein NMR data. *J Am Chem Soc* 132(7):2145–2147.
22. Hyberts SG, Milbradt AG, Wagner AB, Arthanari H, Wagner G (2012) Application of iterative soft thresholding for fast reconstruction of NMR data non-uniformly sampled with multidimensional Poisson Gap scheduling. *J Biomol NMR* 52(4):315–327.
23. Wishart DS, Sykes BD (1994) The 13C chemical-shift index: A simple method for the identification of protein secondary structure using 13C chemical-shift data. *J Biomol NMR* 4(2):171–180.
24. Freissmuth M, et al. (1996) Suramin analogues as subtype-selective G protein inhibitors. *Mol Pharmacol* 49(4):602–611.
25. Sarkar CA, et al. (2008) Directed evolution of a G protein-coupled receptor for expression, stability, and binding selectivity. *Proc Natl Acad Sci USA* 105(39):14808–14813.
26. Schlinkmann KM, et al. (2012) Critical features for biosynthesis, stability, and functionality of a G protein-coupled receptor uncovered by all-versus-all mutations. *Proc Natl Acad Sci USA* 109(25):9810–9815.
27. Egloff P, et al. (2014) Structure of signaling-competent neurotensin receptor 1 obtained by directed evolution in Escherichia coli. *Proc Natl Acad Sci USA* 111(6):E655–E662.
28. Scott DJ, Kummer L, Egloff P, Bathgate RA, Plückthun A (2014) Improving the apo-state detergent stability of NTS1 with CHESS for pharmacological and structural studies. *Biochim Biophys Acta* 1838(11):2817–2824.
29. Egloff P, Deluigi M, Heine P, Balada S, Plückthun A (2015) A cleavable ligand column for the rapid isolation of large quantities of homogeneous and functional neurotensin receptor 1 variants from E. coli. *Protein Expr Purif* 108:106–114.
30. Etzkorn M, et al. (2013) Cell-free expressed bacteriorhodopsin in different soluble membrane mimetics: Biophysical properties and NMR accessibility. *Structure* 21(3):394–401.
31. Hagn F, Etzkorn M, Raschle T, Wagner G (2013) Optimized phospholipid bilayer nanodiscs facilitate high-resolution structure determination of membrane proteins. *J Am Chem Soc* 135(5):1919–1925.
32. Neudecker P, Lundström P, Kay LE (2009) Relaxation dispersion NMR spectroscopy as a tool for detailed studies of protein folding. *Biophys J* 96(6):2045–2054.
33. Loria JP, Berlow RB, Watt ED (2008) Characterization of enzyme motions by solution NMR relaxation dispersion. *Acc Chem Res* 41(2):214–221.
34. Sprangers R, Kay LE (2007) Quantitative dynamics and binding studies of the 20S proteasome by NMR. *Nature* 445(7128):618–622.
35. Lundström P, Vallurupalli P, Religa TL, Dahlquist FW, Kay LE (2007) A single-quantum methyl 13C-relaxation dispersion experiment with improved sensitivity. *J Biomol NMR* 38(1):79–88.
36. Petoukhov MV, et al. (2012) New developments in the program package Atsas for small-angle scattering data analysis. *J Appl Cryst* 45(Pt 2):342–350.
37. Van Der Spoel D, et al. (2005) GROMACS: Fast, flexible, and free. *J Comput Chem* 26(16):1701–1718.
38. Denisov IG, Grinkova YV, Lazarides AA, Sligar SG (2004) Directed self-assembly of monodisperse phospholipid bilayer Nanodiscs with controlled size. *J Am Chem Soc* 126(11):3477–3487.
39. Privalov PL (1979) Stability of proteins: Small globular proteins. *Adv Protein Chem* 33:167–241.
40. Delaglio F, et al. (1995) NMRPipe: A multidimensional spectral processing system based on UNIX pipes. *J Biomol NMR* 6(3):277–293.
41. Schwieters CD, Kuszewski JJ, Tjandra N, Clore GM (2003) The Xplor-NIH NMR molecular structure determination package. *J Magn Reson* 160(1):65–73.
42. Zweckstetter M (2008) NMR: Prediction of molecular alignment from structure using the PALES software. *Nat Protoc* 3(4):679–690.
43. Pettersen EF, et al. (2004) UCSF Chimera–a visualization system for exploratory research and analysis. *J Comput Chem* 25(13):1605–1612.
44. Tollinger M, Skrynnikov NR, Mulder FA, Forman-Kay JD, Kay LE (2001) Slow dynamics in folded and unfolded states of an SH3 domain. *J Am Chem Soc* 123(46):11341–11352.
45. Bieri M, d'Auvergne EJ, Gooley PR (2011) relaxGUI: A new software for fast and simple NMR relaxation data analysis and calculation of ps-ns and μs motion of proteins. *J Biomol NMR* 50(2):147–155.
46. Luz Z, Meiboom S (1963) Nuclear magnetic resonance study of protolysis of trimethylammonium ion in aqueous solution–Order of reaction with respect to solvent. *J Chem Phys* 39(2):366–370.
47. Carver JP, Richards RE (1972) A general two-site solution for the chemical exchange produced dependence of T2 upon the carr-Purcell pulse separation. *J Magn Reson* 6(1):89–105.
48. Humphrey W, Dalke A, Schulten K (1996) VMD: Visual molecular dynamics. *J Mol Graph* 14(1):33–38, 27–28.
49. Phillips JC, et al. (2005) Scalable molecular dynamics with NAMD. *J Comput Chem* 26(16):1781–1802.
50. Laskowski RA, Swindells MB (2011) LigPlot+: Multiple ligand-protein interaction diagrams for drug discovery. *J Chem Inf Model* 51(10):2778–2786.